Characterizing Non-linearities in the Chandra LETG+HRC-S Dispersion Relation

Sun Mi Chung[a], Jeremy J. Drake[a], Vinay L. Kashyap[a], Peter W. Ratzlaff[a] and Bradford J. Wargelin[a]

[a]Chandra X-ray Center, Harvard-Smithsonian Center for Astrophysics, 60 Garden St, Cambridge, MA 02138

ABSTRACT

The dispersion relation for the Chandra Low Energy Transmission Grating Spectrometer (LETGS) is known to better than 1 part in 1000 over the wavelength range 5-150 Å. A recent finding of a data processing software bug that lead to a systematic error in the computation of photon wavelengths has allowed us to trace further discrepancies in the dispersion relation to the boundaries between different microchannel plate segments of the HRC-S imaging detector. However, data acquired during in-flight calibration with the HRC-S detector have always shown the presence of additional non-linear deviations in the positions of some spectral lines by as much as 0.05 Å. These latter effects are thought to be caused by spatial non-linearities in the imaging characteristics of the HRC-S detector. Here, we present an improved dispersion relation for the LETG+HRC-S and new methods to help characterize the spatial non-linearities. We also describe an empirical approach that might be used to help improve the position determination of photon events.

Keywords:

1. INTRODUCTION

Onboard the Chandra X-ray Observatory are two transmission gratings—the High Energy Transmission Grating (HETG) and the Low Energy Transmission Grating (LETG). The Low Energy Transmission Grating Spectrometer (LETGS) (Brinkman et al. 2000) comprises the LETG used in conjunction with the High Resolution Mirror Assembly (HRMA) and one of two focal-plane imaging detectors. The primary detector used with the LETG is the High Resolution Camera spectroscopic array (HRC-S). In this paper, we discuss the dispersion relation of the LETGS+HRC-S combination.

The wavelength coverage of the LETG+HRC-S extends from 1.2 to 170 Å in both positive and negative orders that lie on either side of the 0th order image of the astronomical X-ray source. The dispersion is 1.148 Å/mm and is known to better than 1 part in a 1000, from ∼5 - 150 Å. However, during in-flight calibration, there has been a persistent problem in reconciling the observed dispersion relation with the geometry of the spectrograph itself; in particular, the longer wavelengths appeared to require a significantly larger value of the Rowland diameter than shorter wavelengths. It was also soon discovered that many spectral lines show systematic non-linear deviations in their positions of up to ∼0.05 Å. At a wavelength of 130 Å where prominant spectral lines of Fe in charge states XX-XXIII can be found, this magnitude of deviation corresponds to 115 km s^{-1}. Such a velocity is typical of the particle thermal velocities in an X-ray emitting plasma at several million Kelvin, and is similar to velocities thought to characterise non-thermal motions in astrophysical sources such as stellar coronae. Errors in the LETGS dispersion relation of 0.05 Å are then of some significance.

In the limit of perfect imaging characteristics, the accuracy of the determination of the centroid of a narrow (ie at or close to the instrumental width) spectral line is in principle limited only by signal-to-noise ratio. For many spectral lines seen in astrophysical sources, this limit is much smaller than 0.05 Å. Moreover, the instrument appears stable with a drift over the period of a given astrophysical observation (typically about 100 ks) of only 0.01 Å or less. We are therefore strongly motivated to improve the dominant source of wavelength error. We demonstrate below that this originates in the imaging system, the HRC-S microchannel plate detector.

Further author information: Send correspondence to J.J.D.: E-mail: jdrake@cfa.harvard.edu

We first describe the observations upon which this part of our larger study of the LETG dispersion relation is based, and then discuss the methods of analysis we have applied to elicit the often quite subtle imaging distortions. The results are then compared with an empirical study of the HRC-S "de-gap" correction—the means used to correct event positions for systematic effects in the position determination algorithm—and the degree to which de-gap improvements might ameliorate imaging distortions is qualitatively assessed.

2. OBSERVATIONS

Observations used for the analyses described in this paper are listed in Table 1. Standard CIAO pipeline-processed data were downloaded from the Chandra public data archive.*

Table 1. Observations used in our analyses.

Target Name	ObsID	Exposure [ks]	Start Date	offset [arcmin]
α Aur	1248	85.23	1999 Nov 9 13:27:21	0
α Aur	62435	32.71	1999 Sep 6 00:26:17	0
α Aur	58	34.11	2000 Mar 8 06:29:47	0
α Aur	1009	26.97	2001 Feb 14 11:40:43	0
α Aur	2582	28.83	2002 Oct 4 23:57:53	-1.5
α Aur	3479	30.38	2002 Oct 6 10:01:58	1.5
WZ Sge	2504	20.00	2001 Jul 27 02:30:22	0
AM Her	645	24.11	2000 Sep 30 13:52:40	0
PKS 2155-304	331	63.16	1999 Dec 25	0
PKS 2155-304	1704	26.7	2000 May 31	0
PKS 2155-304	3166	29.97	2001 Jan 04	0
PKS 2155-304	1013	26.82	2001 Apr 06	0

Since the observations listed in Table 1 were carried out at different epochs and calibration regimes, the datasets obtained from the archive are not necessarily uniformly processed. We have therefore reprocessed all of them following the CIAO thread on LETG+HRC-S grating analysis.†

All of the data utilized in our analyses were observed with Normal Mode Pointing (NMP). For observations made with NMP, the Chandra telescope dithers in a Lissajous pattern, distributing photons across multiple detector elements. The amplitude of the dither is nominally 40 × 40 arcseconds, which spans approximately 304 HRC-S 6.43 μm pixels (1.95mm) in both the dispersion and cross-dispersion directions. Section 3.3.2 explains how we take advantage of the dither pattern to compare the dispersion relation at different parts of the detector.

The primary source that was used in our analyses was α Aur (Capella). Capella is an active binary with an emission line spectrum comprised of many bright and narrow lines arising from transitions in highly ionised astrophysically abundant elements (e.g. O, Ne, Mg, Si, S, Fe etc), mostly in the range 5-25 Å, but also including a handful of useful features at longer wavelengths. It is the brightest object of this class in the X-ray sky and is therefore a good target for our calibration analyses involving cross-correlating spectra and determining the positions of narrow lines with accurately known theoretical or laboratory wavelengths. Two of the Capella calibration pointings were designed with aim-points off-set along the dispersion axis by ±1.5 arcmin so as to place bright, strong lines on different detector locations (see "Offset" in Table 1). We also used data from cataclysmic variables WZ Sagittae and AM Herculis. WZ Sge was caught as a target of opportunity during an outburst, and its X-ray spectrum in the LETGS peaked at 120 Å and exhibited useful features for investigating the longer wavelengths covered by the instrument where few lines are to be found in Capella spectra.

*`http://asc.harvard.edu/cda`

†`http://asc.harvard.edu/ciao/threads/spectra_letghrcs`

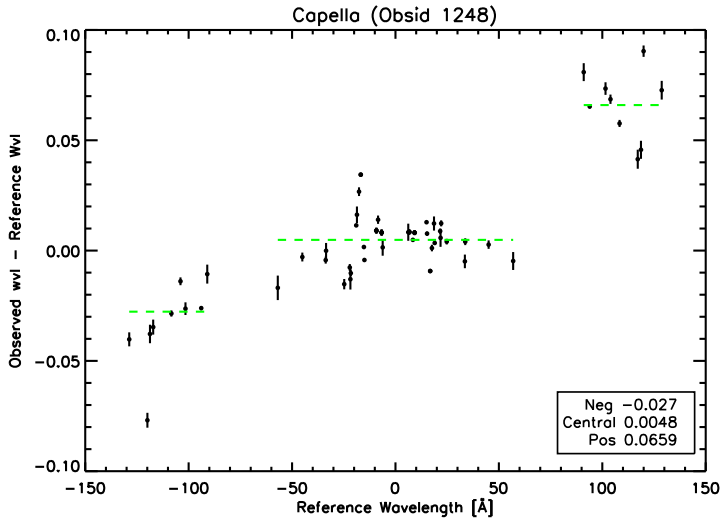

Figure 1. The dispersion relation for the LETG+HRC-S. Dashed lines show the error weighted mean of the data for all 3 HRC-S plates. Note that the outer plates show a signficant wavelength offset from zero. Aside from the wavelength offsets of the outer plates, we also see non-linearities of the dispersion relation along all three plates.

3. ANALYSIS

3.1. Dispersion Relation

The dispersion relation of the LETGS is calibrated and monitored in-flight through observation of cosmic sources with well-understood emission features. In principle, there is only one variable to calibrate: the spectrograph Rowland diameter, which, by the standard grating equation, can be obtained through comparison of the positions of observed features with their theoretical or laboratory wavelengths. In the case of the LETGS, this procedure has proven problematic in that we have until now been unable to produce a unique value of the Rowland diameter for the full wavelength range of the instrument.

The HRC-S detector (Zombeck et al.1995) is a CsI coated microchannel plate design with approximate dimensions 300×20 mm, the long axis of which corresponds to the spectrograph dispersion axis. The detector is split into three microchannel plate segments, each approximately 100 mm long. Soon after launch, it became apparent that the Rowland diameter derived from spectral lines observed on the central plate ($\lambda \leq 50$ Å or so) did not appear to match that required for the two outer plates. These outer plates suggested a diameter 0.05% larger—a small but significant difference important for the correct interpretation of observed spectra. Thorough investigation of all hardware systems involved failed to find an explanation for this effect. It was recently discovered, however, that the largest part of this was due to numerical improprieties in processing software. The dispersion relation after correction of this problem is illustrated in Figure 1. In this figure, lines that fall on the outer HRC-S plates still show significant systematic offset, such that the observed wavelength positions are larger than the known reference wavelengths. We can now understand these systematic offsets in terms of errors in the effective sizes of the gaps between microchannel plate segments; these data can be used to correct the effective plate gaps such that the dispersion relation is essentially flat across the whole wavelength range of the instrument. Once the data are reprocessed with suitably decreased plate gaps, the outer plates no longer show the systematic wavelength shift (Figure 2).

Prominent in Figure 2, however, are large departures from the otherwise flat dispersion relation. These correspond to spectral lines whose observed positions are significantly different to their predicted positions. Despite these extraneous points, the standard deviation in predicted vs observed wavelengths across the entire wavelength range amounts to only 0.0129 Å, or slightly better than 1 part in 10,000.

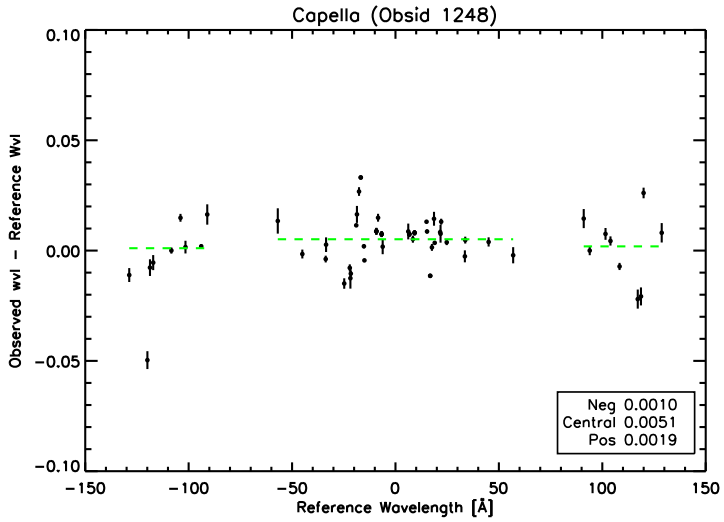

Figure 2. The dispersion relation for the LETG+HRC-S after plate gaps were reduced. The error weighted mean for the three plates are still non-zero, but this is attributed to random errors from the non-linearities, rather than systematic errors.

3.2. Non-linearity

Dispersion anomalies illustrated by Figure 2 first came to light soon after early in-flight calibration data were received on the ground when spectra from + and − orders were compared. While in some spectral regions overlap was very good, in others there was a visible mis-match. We show a similar effect for the LETG+HRC-S spectrum of Capella in Figure 5. Instead of comparing + and − orders, here we show the −1 order spectra corresponding to only those times when the source was at opposite sides of the dither pattern: at any given wavelength, the two spectra are from detector regions separated by about 1.5mm. While near 14 Å the overlap is good, there is an increasing mismatch going toward longer wavelengths, with the largest effect seen near Fe XVIII 16.78 Å. Such discrepancies can only be understood in terms of non-linearity in the imaging system.

3.3. Cross-correlation

One way we can characterize the non-linearities of the LETG+HRC-S dispersion relation is to cross-correlate spectra extracted from events that fall on different parts of the detector. In a spectrograph with perfectly linear imaging characteristics in the dispersion axis, the spectra from both + and − orders should overlap perfectly, as should spectra extracted from times when the spacecraft was pointing within two particular regions of the lissajous dither pattern. Cross-correlation provides a way to test where the overlap between two spectra from different detector regions is good or bad and can serve to highlight problem areas.

We designate one spectrum as the 'reference', to which the second spectrum is compared. By shifting one spectrum relative to the reference spectrum, and computing a correlation coefficient at each shift, we can determine at which shift the two spectra are best matched. There are various ways of computing such a correlation signal. In our case, we have computed the χ^2 value at each shift:

$$\chi^2 = \sum \frac{(C_{ref}(\lambda) - C_2(\lambda+\delta\lambda))^2}{\sigma_{ref}(\lambda)^2 + \sigma_2(\lambda+\delta\lambda)^2}; \quad \lambda - \Delta\lambda \leq \lambda \leq \lambda + \Delta\lambda \tag{1}$$

where $C_{ref}(\lambda)$ and $C_2(\lambda+\delta\lambda)$ are the two spectra being compared, in the form of counts/0.0125 Å, and $\sigma_{ref}(\lambda)$ and $\sigma_2(\lambda+\delta\lambda)$ are the respective errors. These quantities are then summed over a window region. The parameter $\delta\lambda$ represents the offset between the two spectra at which the test statistic is computed, and $\Delta\lambda$ is the wavelength interval over which the spectra are compared. This last parameter needs to be sufficiently large that enough

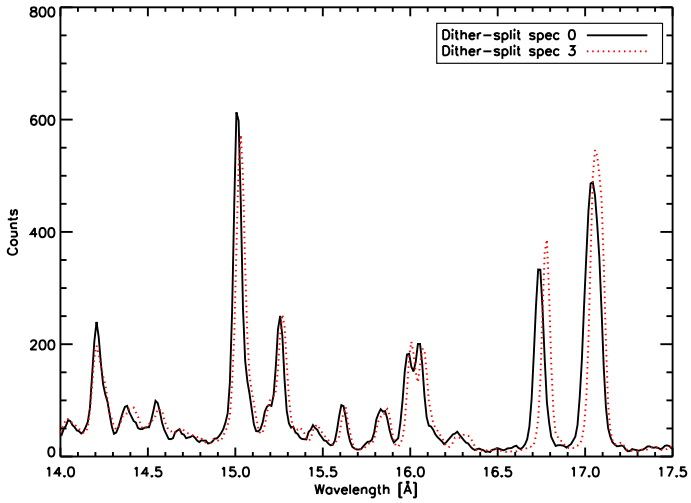

Figure 3. Negative order Capella spectra extracted from times when the source was at opposite ends of the dither pattern are overplotted to illustrate the non-linearities of the dispersion relation along the detector. At each wavelength, the spectra represent data taken from detector regions approximately 1.5mm apart. Note the good alignment near 14 Å and the trend of increasing mismatch toward longer wavelengths.

signal is included, but sufficiently small as to usefully probe the scale size of the distortions. Typically, we have adopted a value of 1.2 Å. We use the Gehrels approximation to estimate the errors on the observed counts in the spectra. In order to obtain the uncertainty on the value of $\delta\lambda$ that corresponds to the minimum χ^2, we have utilized a Monte-Carlo method in which we randomize the noise on $C_2(\lambda)$ N number of times, (where $N \sim 10-20$), and cross-correlate the reference spectrum with each of the randomized data sets. The uncertainty is then obtained from the distribution of the minima thus produced.

We have used this method in an attempt to map out the relative distortions between the positive order and negative order spectra and also to compare spectra taken from different parts of the dither pattern, which correspond to different parts of the detector.

3.3.1. Positive vs Negative Orders

To estimate the magnitude of the relative distortions between opposite sides of the detector, we cross-correlated negative with positive orders as described above in section 3.3. Cross-correlation was repeated 15 times for 15 randomized $C_2(\lambda)$ data sets. We used a cross-correlation window size of $\Delta\lambda = 1.2$ Å and computed χ^2 at intervals of 0.003Å. The $\Delta\lambda$ window was stepped through the spectrum with a step size of 0.12 Å. Figure 4 shows the relative wavelength shifts as a function of wavelength between the negative and positive orders that are required to minimise the test statistic for an observation of Capella (ObsID 1248).

It is clear from Figure 4 that there are relative distortions between + and − orders amounting up to 0.05 Å. To put this into perspective, this is about the same size as the full width at half maximum of instrumental profile. While Figure 4 does not illustrate this very well because of scant data on the outer plates, the distortions here appear larger than on the central plate in observations such as WZ Sge.

3.3.2. Dither-Splitting

While the + vs − order comparison is very useful for diagnosing the presence of non-linearities, this test leaves the ambiguity as to in which order the distortions arise. We therefore devised another test that uses the fact that the dither pattern trails any given narrow spectra feature over a 2 mm square region of the detector. By splitting up the events of an observation by times corresponding to when the telescope was pointing at a particular region of the dither pattern, we are then able to search for distortions on the dither pattern size scale. To achieve this,

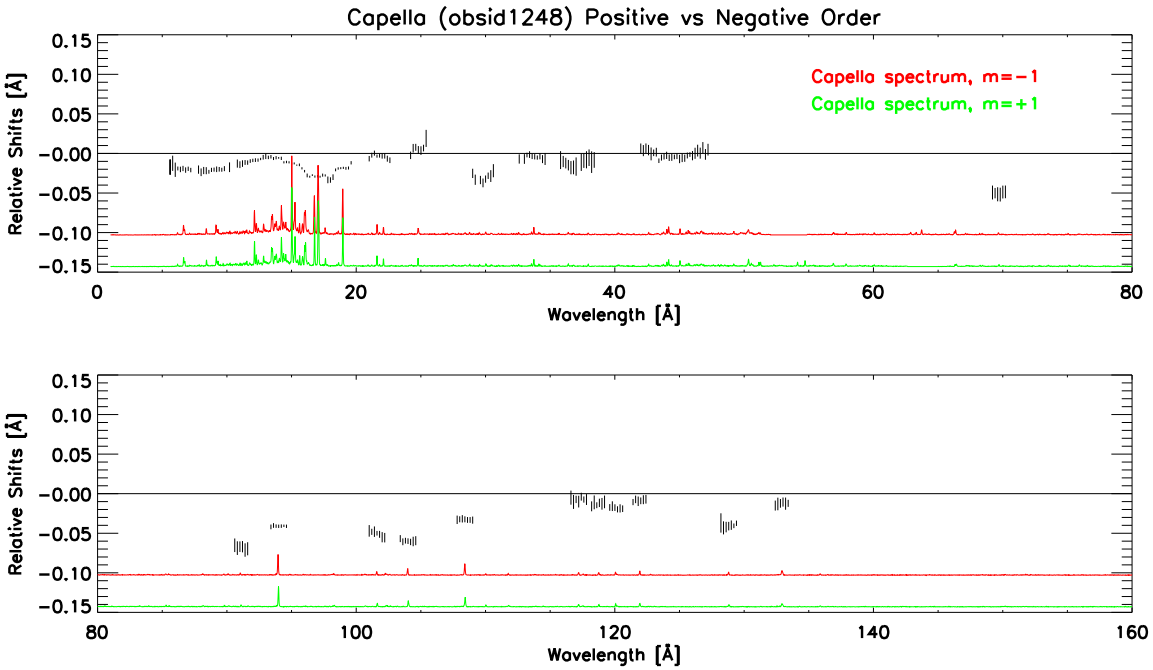

Figure 4. Relative wavelength shifts between the negative order and positive order spectra of Capella. The two spectra which were cross-correlated against each other are also shown, displayed on an arbitrary intensity scale.

we typically split the dither pattern into four regions in the dispersion direction. A given narrow line taken from events selected from one side of the dither is then imaged over a region of the detector that is separated by approximately 1.5 mm from the same line seen in events from the opposite side of the pattern.

Time filters to be used to split events by dither location were generated based on the observatory pointing aspect telemetry. The "dither-split" spectra were then extracted from the time-filtered event lists using the CIAO tool `tgextract`. Splitting the dither pattern into 4 parts effectively reduces the total number of counts in each spectrum to 25% of the original signal. In order to increase the signal to noise ratio (S/N), we coadded data from observations whose aimpoints were approximately the same. These observations are those with offset=0 listed in Table 2. We computed the test statistic at intervals of 0.003 Å, using again a value of $\Delta\lambda = 1.2$ Å. In turn, this $\Delta\lambda$ window is stepped along the spectrum at intervals of 0.12Å. At each of these steps $C_2(\lambda)$ is shifted from -0.15 to +0.15 Å relative to the reference spectrum to ensure that deviations as large as 0.1 Å are not missed. We repeat this process for 15 randomized data sets, generated by randomizing the noise on $C_2(\lambda)$, as described in section 3.3.

The results of the dither-splitting analysis for the coadded on-axis observations of Table 2 are illustrated in Figure 5. These results correspond to data taken from opposite sides of the dither and are interesting because they confirm that *the distortions occur on scales similar to or smaller than the size of the dither pattern.* The − order distortions appear to be larger than those seen in the + order, and there is a clear correspondence between the distortions seen in the the − order and those seen in the + and − order comparison in Figure 4. Again, based on the limited information here, it appears that the distortions are larger on the outer plates at wavelengths $\lambda > 50$ Å.

3.4. Line Centroiding

By looking at the event list in a coordinate system defined by the observed line wavelength, λ, and the dispersion direction of the detector (detx), we can actually see the spatial non-linearities in the light of bright lines. A line seen in this coordinate system should look like a horizontal straight line, the horizontal extent of which is

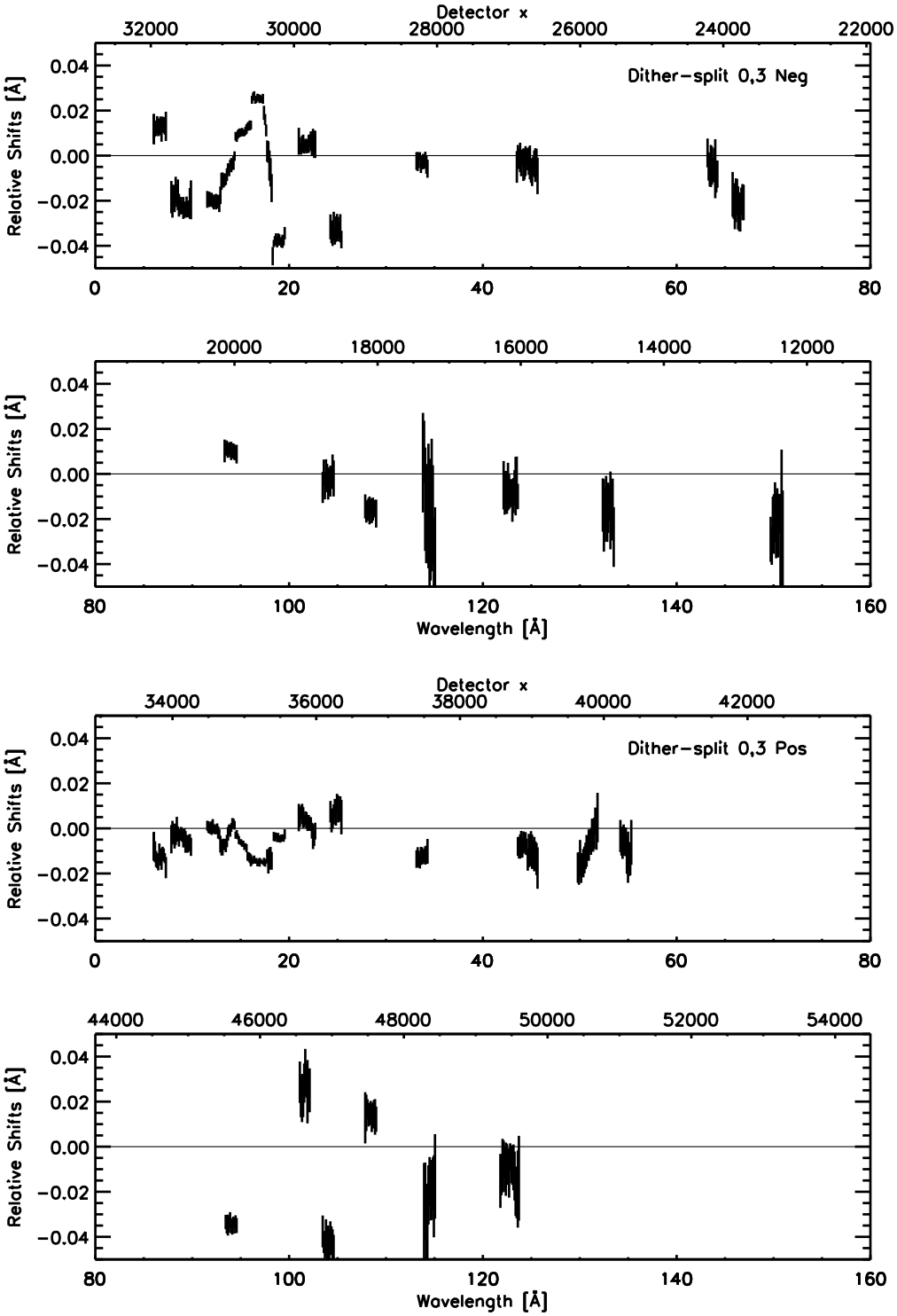

Figure 5. Illustration of the wavelength distortions between different parts of the dither pattern for negative order spectra (upper plot), and for positive order spectra (lower plot). We show results from cross-correlation of spectra extracted from opposite sides of the dither pattern.

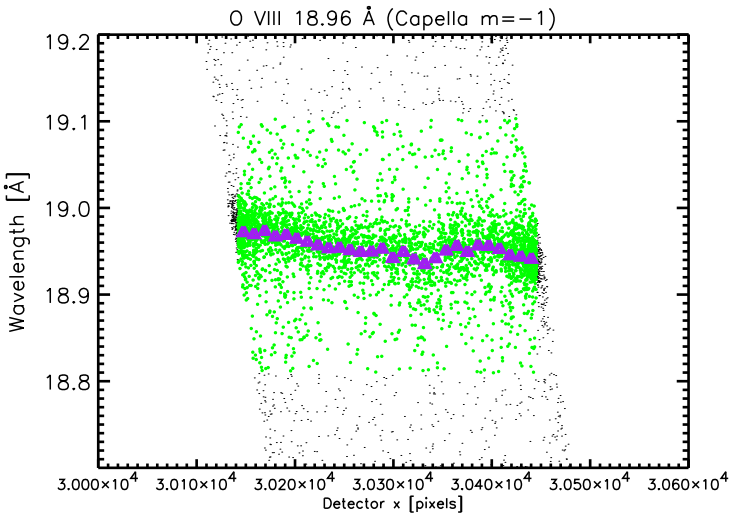

Figure 6. Events from the OVIII line of the negative order of Capella (obsid 1248), shown in λ-detector x space. Also shown (triangles) are the measured wavelength centroids of the events at different locations on the detector dispersion direction.

determined by the size of the dither pattern projected onto the detx axis. Figure 6 shows the events of the OVIII Lyα resonance line near 19 Å plotted in λ,detx space. Since we expect no significant velocity shifts of this line, the "wobble" seen here must be caused by imaging distortions. We can then map out the non-linearities of the dispersion relation along detx by determining the centroid of events in the λ axis, in small steps of detx, and by comparing these observed centroids with the known rest line wavelengths. These centroids are also illustrated in Figure 6.

The drawback to this analysis is that it only works for relatively strong emission lines, thereby limiting the area of the detector over which we can map out the distortions. Relatively strong lines are necessary because each line is split up into bins of detx, and centroids are measured for the events in each bin. The number of detx bins can of course be varied from line to line, and to maintain a constant S/N ratio is proportional to the total flux of the line. Weaker lines therefore result in lower effective resolving power for discerning detector distortions.

Figure 7 illustrates the results of such an analysis as applied to bright lines seen in 3 separate Capella observations. Here, we have utlised the observations obtained from pointings offset from the nominal aim point by $\pm$1.5 arcminutes in order to place bright lines on different detector regions (ObsIDs 2582 and 3479).

Interpreting results from this line-centroiding analysis is somewhat more straightforward than for the cross-correlation analysis. Whereas wavelength distortions obtained from cross-correlating spectra are always relative to the reference spectrum used, the line-centroiding analysis provides a more direct vision of the distortions. Again, in Figure 7 we see evidence for larger distortions on the outer plates, though we caution that this analysis was performed prior to the correction of the plate gaps and the systematic wavelength calibration errors for the outer plates are included (Figure 1).

4. POSSIBLE PROGRESS THROUGH "DE-GAP"?

The position-sensitive charge detector is a hybrid system in which one axis is comprised of parallel wires, while the other is comprised of a system of parallel gold tracks deposited on a ceramic substrate (Murray et al.1989).

Every eighth wire or track is connected to a charge-sensitive amplifier (referred to as a "tap"), and charge cloud positions resulting from photon events are estimated by the distribution of charge seen by the nearest three taps. This "three tap algorithm" works sufficiently well to locate the event within 10-20 microns of the true position, but an artifact is that gaps are produced in images half way between taps.

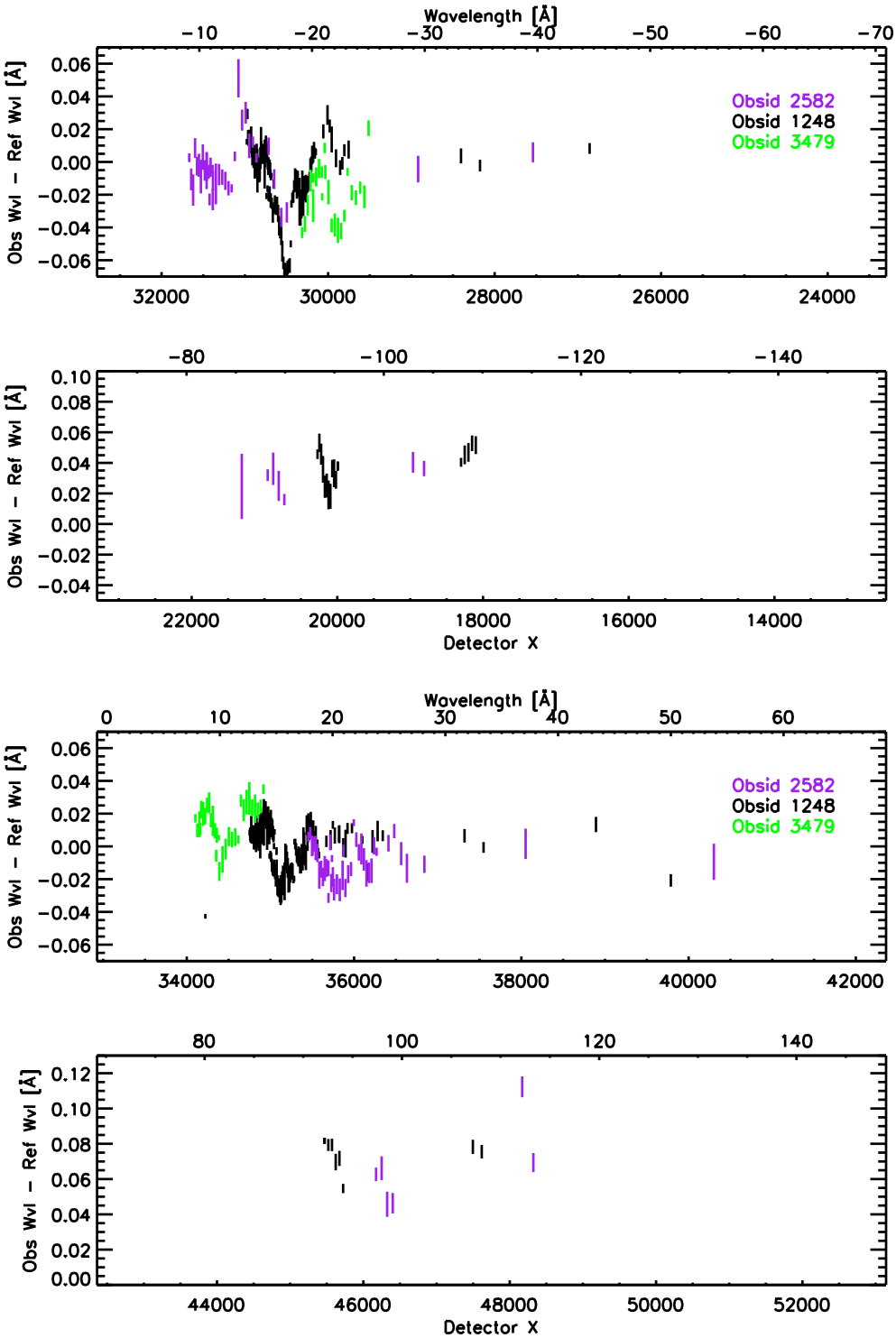

Figure 7. Illustrations of the difference in observed versus known reference wavelengths, determined by centroiding events along different locations in the detx direction. We have used 3 Capella observations with different offsets, to map out distortions along a more extended region of the detector.

The exact characteristics of these gaps depend on the details of the charge cloud distributions and amplifier responses, the former of which can be complicated and have significant spatial dependence over the detector. A phenomenological correction—referred to as the "de-gap" correction—to adjust the event positions and fill in the gaps has been derived from laboratory data and is implemented in standard processing.

However, inspection of in-flight data has revealed some problems with this correction. Faint "ghost" images of gaps sometimes remain in in-flight data. Moreover, we have now devised a method to derive an empirical de-gap correction based on in-flight observations of strong featureless continuum sources and find significant differences between this correction and that applied by the current de-gap method. We use the observed spectra to estimate the true distribution of counts across each tap (including the effects of aspect dither), and constrain the observed distribution of counts to follow this true distribution. The adjustment to event positions is required to ensure that the distribution of counts indeed follows that expected from the empirical de-gap correction.

Since the de-gap correction involves adjustment of photon event positions, it is quite likely that problems in the de-gap correction could be responsible for some of the detector distortions we are seeing. To determine whether or not this might be the case, we can compare the magnitude of the position corrections using both schemes and examine whether or not there are significant differences in detector regions prone to imaging non-linearities. In Figure 8, we illustrate the *difference* between the event position correction for the standard degap map and our own event position correction derived using the largely featureless continuum source PKS 2155-304 (see Table 1). Because this is done in detector coordinates and sources are dithered, we have convolved the difference in corrections with the dither profile—the integrated time spent at each phase of the pattern as projected onto the dispersion axis.

Under the assumption that our degap map is the correct one, the data illustrated in Figure 8 should correspond to the distortion in the wavelength scale that arise as a result of improprieties in the current de-gap map applied in data processing. To determine in a qualitative sense whether or not these distortions correspond to those that we are seeing in the instrument, we also show in Figure 8 the deviations from the predicted positions of bright emission lines seen in the spectra of Capella (ObsID 1248). Based on this figure, it is clear that the large deviation in evidence in the $-$ order between 15 and 20 Å does not have a significant counterpart in the de-gap distortion. However, some deviations in line positions do seem to line up with predicted deviations resulting from de-gap. Qualitatively, we see that larger de-gap distortions are predicted for the outer plates. Partly this could be related to the spectrum of PKS 2155-304, whose observed counts per unit wavelength bin do decline toward longer wavelengths as a result of interstellar medium absorption and decreasing instrument effective area. Nevertheless, we are encouraged by this comparison that at least some of the distortions we are seeing are de-gap related.

5. CONCLUSIONS

Substantial progress has been made in understanding salient problems with the LETG+HRC-S dispersion relation seen soon after the launch of *Chandra*. Through empirical adjustment of the HRC-S microchannel plate gaps we have been able to produce a dispersion relation to which observed spectral lines adhere with a standard deviation of only 0.019 Å, or to better than 1 part in 10,000. Significant non-linearities in the dispersion relation remain that can amount up to 0.05 Å—the size of the instrumental width—and that hamper the scientific analysis of observed spectra.

We have performed an empirical study of the detector de-gap correction using in-flight observations of a strong continuum source. Our empirical de-gap correction suggests that at least some of the observed distortions arise as a result of errors in the current de-gap correction derived pre-launch from laboratory data. Our results highlight problems with the current de-gap on the outer plates, and suggest that improvements in the degap correction can lead to significant improvements in the dispersion relation. Some distortions, such as that between 15 and 20 Å in the -1 order are apparently not caused by de-gap errors and we must seek alternative solutions to remedy the problem.

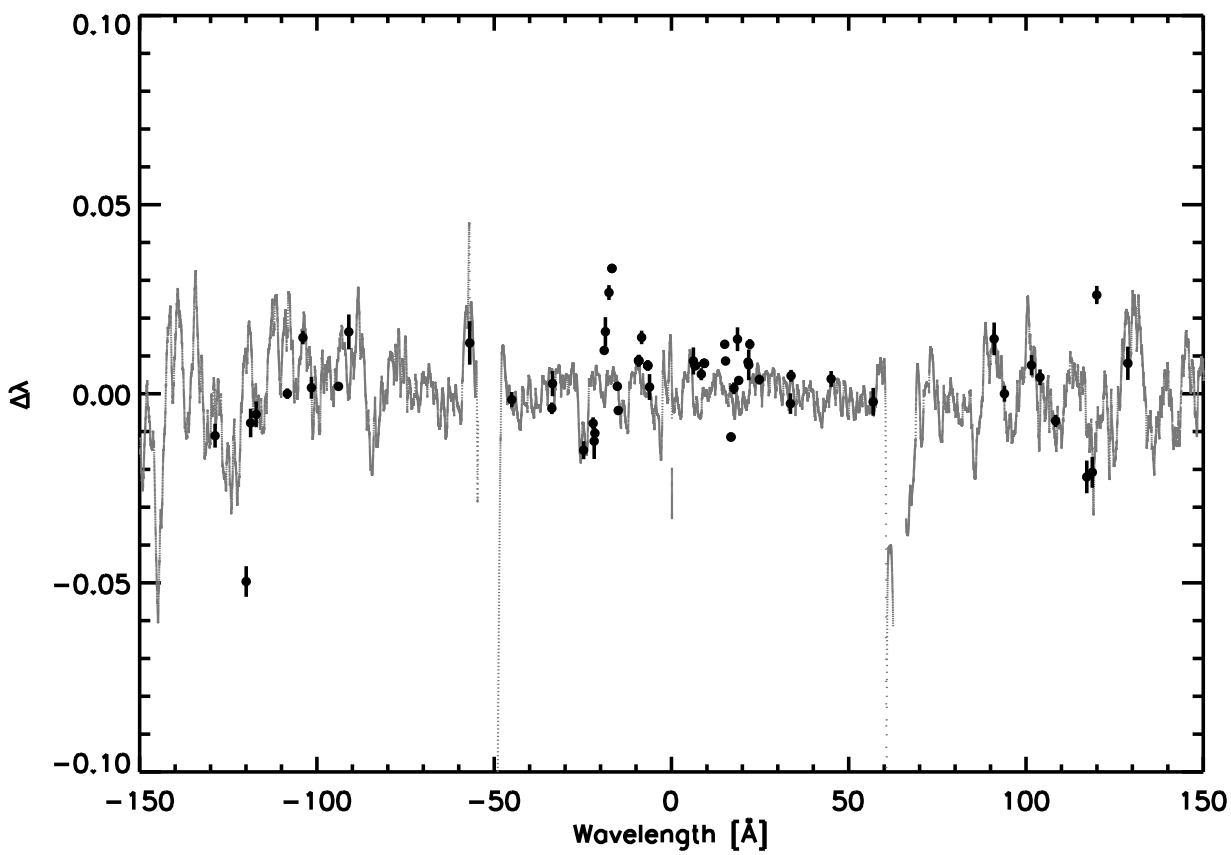

Figure 8. The difference between our empirical de-gap event position correction derived using observations of the relatively featureless continuum of the blazar PKS 2155-304 and the current standard de-gap correction, convolved with the dither kernel projected onto the dispersion axis. This difference shows the distortions that could arise as a result of errors in the current de-gap correction. Over-plotted on these data we show the deviations of the centroids of bright emission lines seen in Capella from their predicted values.

6. ACKNOWLEDGEMENTS

This work was supported by NASA contract NAS8-39073.

REFERENCES

1. M. Zombeck et al.," High-resolution camera (HRC) on the Advanced X-Ray Astrophysics Facility (AXAF) " *Proc. SPIE* **2518**, pp. 96-106, 1995
2. A. Brinkman et al.," First Light Measurements of Capella with the Low-Energy Transmission Grating Spectrometer aboard the Chandra X-Ray Observatory " *ApJ* **530**, pp. L111-L114, 2000
3. S. Murray et al.," Position Modeling for the AXAF High resolution Camera (HRC)" *Proc. SPIE* **1159**, pp. 460-475, 1989